Research Article

A synergistic pH-responsive serum albumin-based drug delivery system loaded with doxorubicin and pentacyclic triterpene betulinic acid for potential treatment of NSCLC.

Zally Torres-Martinez1, Daraishka Perez2, Grace Torres3, Sthephanie Estrada4, Clarissa Correa3, Natasha Mederos3, Kimberly Velazquez3, Betzaida Castillo5, Kai Griebenow1,*, Yamixa Delgado3,*

1 Chemistry Department, University of Puerto Rico-Rio Piedras Campus, San Juan PR, USA
2 Neuroscience Department, Universidad Central del Caribe, Bayamon PR, USA
3 Biochemistry & Pharmacology Department, San Juan Bautista School of Medicine, Caguas PR, USA
4 Biology Department, University of Puerto Rico-Cayey, Cayey PR, USA
5 Chemistry Department, University of Puerto Rico-Humacao, Humacao PR, USA
* Correspondence: K.G. kai.griebenow@gmail.com, Y.D. ydelgado@sanjuanbautista.edu ; Tel.: (optional)

Abstract: Nanosized drug delivery systems (DDS) have been studied as a novel strategy against cancer due to their potential to simultaneously decrease drug inactivation and systemic toxicity and increase passive and/or active drug accumulation within the tumor(s). Triterpenes are plant-derived compounds with interesting therapeutic properties. Betulinic acid (BeA) is a pentacyclic triterpene which has great cytotoxic activity against different cancer types. Herein, we developed a nanosized protein-based DDS of bovine serum albumin (BSA) as the drug carrier combining two compounds: doxorubicin (Dox) and the triterpene BeA using an oil-water-like micro-emulsion method. Spectrophotometric assays were performed to determine protein and drug concentrations in the DDS. The biophysical properties of these DDS were characterized using dynamic light scattering (DLS) and circular dichroism (CD) spectroscopy confirming nanoparticle (NP) formation and drug loading into the protein structure, respectively. The encapsulation efficiency was 77% for Dox and 18% for BeA. More than 50% of both drugs were released within 24 h, at pH 6.8, while less drug was released at pH 7.4 in this time period. Co-incubation viability assays of Dox and BeA alone for 24 h demonstrated synergistic cytotoxic activity in the low μM range against the non-small cell lung carcinoma (NSCLC) A549 cells. Viability assays of the BSA(Dox+BeA) DDS demonstrated a higher synergistic cytotoxic activity than the two drugs with no carrier. Moreover, confocal microscopy analysis confirmed cellular internalization of the DDS and nucleus accumulation of the Dox. We determined the mechanism of action of the BSA(Dox+BeA) DDS, confirming S-phase cell cycle arrest, DNA damage, caspase cascade activation, and downregulation of the epidermal growth factor receptor (EGFR) expression. This DDS has the potential to synergistically maximize the therapeutic effect of Dox and diminish chemoresistance induced by EGFR expression using a natural triterpene against NSCLC.

Keywords: Betulinic acid; bovine serum albumin; doxorubicin; drug delivery system; lung cancer; synergistic effect.

1. Introduction

For decades, chemotherapy has been the treatment of choice for many cancer patients. However, there is no gold-standard therapeutic approach to eradicate cancer. This prompts the development of new strategies for more specific treatments design depending on the diagnosed cancer type [1]. Considering that chemotherapy affects all growing cells, lack of tumor specificity is one of the biggest drawbacks in cancer treatments due to severe toxic side effects. Furthermore, the acquired chemoresistance produced more aggressive cancer cells in patients under treatment. To tackle these problems, development

of nanosized DDS has been an emerging strategy to treat cancer as well as other diseases that need more target-specific treatments [2-4].

Doxorubicin (Dox), a natural anthracycline, is a chemotherapeutic drug recommended for several types of cancer, e.g., small cell lung carcinoma (SCLC)[2]. However, Dox is not curative to non-small cell lung carcinoma (NSCLC) [3] and also induces resistance, diminishing its therapeutic effects [4]. The mechanism of action of Dox promotes inhibition of the DNA topoisomerase in RNA/DNA synthesis and an increase in reactive oxygen species [5]. In addition, Dox also induces chemoresistance by the activation of epidermal growth factor receptor (EGFR) [6]. Due to the lack of selectivity and chemoresistance, patients undergoing Dox treatment may experience cardiac toxicity and cancer recurrence [5] [7].

Betulinic acid (BeA), the other compound investigated herein, is a lupine-type pentacyclic triterpene mainly isolated from birch trees, is a phytochemical compound with a great potential against several diseases. Some multifunctional aspects include antimicrobial, antiviral, anti-inflammatory and anticancer activities [8, 9]. The anticancer properties of BeA have shown potent cytotoxic activity against various types of cancer *in vitro* and *in vivo* [10]. In addition, researchers have reported BeA antitumor mechanism through mitochondrial oxidative stress induction, regulation of SP transcription factor Sp1 (specificity protein 1, a protein encoded by SP1 gene), and inhibiting proliferative factors mediating tumor cell death [10]. However, an essential disadvantage of BeA, which limits its biomedical use to a greater extent, is its poor water solubility of only 0.02 μg/ml at room temperature [8]. To improve this, researchers have studied different encapsulation methods, including self-assembling properties, to enhance BeA bioavailability under physiological conditions [11, 12]. Thus, several benefits arise from drug combinations working in synergy including toxicity decrease and fewer side effects compared with higher doses of single drugs [13, 14]. Hence, combining BeA with other drugs could work as an excellent alternative anticancer treatment.

The most abundant plasma protein is serum albumin (SA), a highly water-soluble and stable protein over a wide pH range (from pH 4 to 9). SA possesses many interaction sites (e.g., pockets) and functional groups (e.g., amines and carboxyls) ideal for covalent modification, and molecule- (polar and non-polar) and ion-loading [15]. Also, the flexibility of the SA structure , facilitates the binding of different compounds [15]. Interestingly, SA has a primary and three-dimensional structure highly conserved in mammals, e.g., the bovine SA has 76% amino acid similarity with human SA [16]. HSA and BSA-based DDS have shown many advantages over the "naked" drugs, including a better NP size, homogeneity, storage and physiological stability, solubility and dispersion in aqueous solution, biocompatibility, biodegradability, and the possibility of surface modification leading to more specific therapy [17]. Moreover, cancer cells overexpress various albumin receptors (i.e., gp60 and SPARC) which can contribute to enhanced albumin-based nanoparticle uptake [18]. Specifically, Abraxane (albumin-based nanoparticles containing paclitaxel) shows improved drug efficiency over Taxol (paclitaxel) [19].

In this work, we encapsulated a drug combination of BeA and Dox in a BSA-based DDS using a cost-effective oil-in-water-like emulsion method. The resulting nanosized DDS was characterized and the drug-release in tumor-like and in normal physiological environments determined. The effect of the BEA and Dox loaded DDS and the isolated drugs on NSCLC A549 cell viability was measured and analyzed for synergistic interactions. Additionally, the drug effect on the metabolic activity of the treated A549 cells were investigated.

2. Materials and Methods

2.1 Chemicals and Reagents

Fatty acid free bovine serum albumin (BSA), betulinic acid (BeA), and doxorubicin (Dox) were purchased from Sigma-Aldrich (St. Louis, MO). The cell lines A549 (human lung adenocarcinoma; ATCC® CCL-185™) and MRC5 (human fibroblast-like; ATCC CCL-171™) were from the American Type Culture Collection (Manassas, VA). CellTiter 96 aqueous non-radioactive cell proliferation assay (3-(4,5-dimethylthiazol-2-yl)-5-(3-carboxymethoxyphenyl)-2-(4-sulfophenyl)-2H-tetrazolium (MTS) reagent) was from Promega Corporation (Madison, WI). NucBlue® Fixed Cell Ready Probes® Reagent (4',6-diamidino-2-phenylindole dihydrochloride, DAPI), fluorescein (FITC), and Vybrant™ DiO Cell-Labeling Solution were purchased from Thermo-Fisher Scientific (Waltham, MA). Cell cycle, caspase-3, DNA damage, and ROS assay were from Luminex Corporation (Austin, TX). All other chemicals (analytical grade) were purchased from various suppliers and used without further purification.

2.2 Preparation of the nanosized DDS

Protein-based DDS were designed using an oil-in-water-like emulsion following a nanoprecipitation step. Protein NPs were obtained following a procedure with several adaptations as described by Molina et al. 2016, and Delgado et al. 2015 [20, 21]. DDS synthesis was optimized by adjusting several parameters. Briefly, BSA was dissolved in a 1X phosphate buffer solution, pH 7.4, to achieve a final concentration of 5 mg/ml at 40ºC. The two drugs, BeA and Dox, were dissolved in N, N-Dimethylformamide (DMF) and then, the solvent was added with a syringe needle at a constant flow of 120 ml/h to the BSA solution to achieve a final concentration ratio of 1:2 protein:drug (w:w). The dispersed emulsion was left stirring at a constant rate of 100 rpm for 4 h. Afterward, this preparation was centrifuged thrice with nanopure water using a 10 kDa filter unit at 5,000 rpm for 10 min to remove the unattached free drug moieties. The final DDS solution was freeze-dried for 48 h and stored at -20 ºC until further use.

2.3 Characterization of the DDS

2.3.1 Quantification of the DDS components

Spectrophotometric measurements were implemented to determine the concentration of each component in the DDS. The standard protocol using the Bradford Coomassie reagent was utilized to determine the BSA protein concentration in the DDS from the absorbance at 570 nm [22]. A calibration curve was constructed with BSA standards. An aliquot of 5 μl was analyzed spectrophotometrically following the Bradford Coomassie protocol. The nanoparticular yield was then calculated as follows:

NPs yield= (amount of BSA in solution / initial amount of BSA) x 100

The Dox concentration was determined using its intrinsic absorbance at 485 nm [23]. For the determination of the BeA, we selected to use the vanillin-sulfuric acid assay [24]. In brief, we prepared several dilutions from a BeA stock solution in ethanol (5 mg/ml) for a calibration curve.   The dilutions and the DDS samples were heated at 85 ºC for solvent evaporation. Afterwards, 250 μL of vanillin stock (50 mg/ml) were added followed by addition of 500 μl of sulfuric acid (95.0-98.0%) to each sample. Then, the solutions were heated at 60 ºC for 30 min. Subsequently, the solutions were transferred into an ice bath. Then, 2 ml of acetic acid (99.7%) were added and incubated for 20 min. Once room temperature was reached, the DDS samples and triterpene dilutions were measured at 548 nm. For these colorimetric assays, we used the Thermofisher Scientific Multiskan FC microplate reader spectrophotometer.

2.3.2 Encapsulation efficiency (EE) and NPs yield

An aliquot of 20 μl of the DDS was collected to determine the concentration of each drug. The final amount of each drug in the DDS was obtained as explained before for the quantification of Dox and BeA. The equation used to calculate this parameter is [1]:

% EE= ((final drug weight in DDS)/ (Initial weight of drug for DDS preparation)) x 100

The nanoparticle yield was calculated by using the equation [18]:

NPs yield: ((amount of BSA in nanoparticle)/ initial amount of BSA) x 100

2.3.3 Particle size, polydispersity and zeta potential

The DDS size, polydispersity index, and zeta potential were measured using a dynamic light scattering (DLS) instrument (Mobius model, Wyatt Technology, California, USA). Samples were dissolved in nanopure water and placed in a quartz cuvette for the measurements. Each value is an average of three runs of around comprised of 13 measurements each.

2.3.4 *In vitro* drug release studies

Drug release experiments were conducted as described by Morales-Cruz et al. [25]. Briefly, one ml of a 5 mg/ml solution of the DDS in 25 mM sodium bicarbonate at pH 6.8 and 7.4, was incubated at 37 ºC under stirring. At pre-determined time intervals (typically 24 h), the DDS sample was filtered through a centrifugal filter device at 12,500 rpm for 15 min. The filtrated solution (with the released drug) was measured at 470 nm (Dox intrinsic absorbance) after the filtration through the centrifugal filter device. Also, from the filtered solution the BeA component was quantified using the vanillin-sulfuric acid assay as described in section 2.3.1. To maintain sink release conditions, the DDS was re-suspended in 1 mL of bicarbonate buffer. The data are presented as accumulative release profiles of an average triplicate and the standard deviations were calculated.

2.4 Cell culture experiments

2.4.1 Cell culture conditions

NSCLC A549 and human normal lung MRC5 cell lines were maintained following ATCC protocols.   These cells were cultured in supplemented Dulbecco's Modified Eagle's Medium (DMEM, containing 1% L-glutamine, 10% fetal bovine serum (FBS), and 1% penicillin/streptomycin). Cells were kept in a humidified incubator under 5% CO_2 and 95% air at 37°C. All experiments were conducted before cells reached 25 passages. For cell viability experiments, A549 and MRC5 cells were seeded in 96-well plates for 24 h.

2.4.2 Cell viability

A549 and MRC5 cells were seeded into 96-well plates at a density of 1 x10^5 cells/well in 0.1 ml supplemented DMEM medium. After 24 h, cells were treated with various concentrations (10, 25, 50, 75, 100 mg/ml) of BSA-(Dox+BeA) DDS and controls (BSA DDS, BSA-BeA, BSA-Dox) and incubated for 24 h. Then, 10 ul of the MTS reagent from CellTiter 96® Aqueous Non-Radioactive Cell Proliferation Assay (Promega G5421) was added to each well. Then, the plate was incubated at 37 ºC and 5% CO_2 atmosphere for 1 h. After incubation, absorbance was measured at 492 nm in a microplate reader (Mean ± SD, n=8). The cell viability was calculated as follows:

% Viability = (sample data – incubation media data)/(untreated cells data – incubation media data) X 100

The 50% inhibitory concentration (IC_{50}) was calculated by Graphpad Prism 9 software.

2.5 Synergism, additive or antagonistic drug interactions

To evaluate the cytotoxic interactions of the BeA and Dox combination, A549 cell viability was measured with different concentrations of Dox and BeA by the MTS reagent. The absorbance was measured at 492 nm after 1 h of incubation. The cell viability was calculated from a quadruplicate sample group. The concentration index (CI) was calculated by CompuSyn software based on the Chou and Talalay [26] equation.

CI=D1/Dx1+D2/Dx2

In the formula, Dx1 or Dx2 is the drug dose alone with the inhibition on x%, and D1 or the D2 is the portion of the drug in combination with the same inhibition on x%. After the interaction of different drugs is determined, the CI value can be obtained. Depending on the CI the drug interactions can be described as synergism, antagonism, or additive effect. A CI of 1 indicates additive effects in the drug combination studied, a CI of <1 indicates synergism while a CI of >1 indicates antagonism.

In addition, Synergy Finder 2.0 software was used to determine a synergy score for combination therapy [27]. Synergy Finder 2.0 is an open and free software that implements an efficient synergy estimation for multi-drug combinations, novel visualization, and statistical treatment of replicate measurements among other features to determine synergism in drug combinations. When the synergy score is larger than 10 it indicates a synergistic effect; if the score is less than -10 it indicates an antagonistic effect; if the score is between -10 to 10 the interaction between the drugs is additive.

2.6 Cellular internalization of DDS

The DDS were labeled with fluorescein isothiocyanate (FITC) to visualize cellular internalization using confocal microscopy.

2.6.1 DDS-FITC labeling.

Controls (BSA) and samples (BSA-(Dox+BeA) DDS) were labeled with FITC by 24 h of incubation. In brief, the DDS was dispersed at 2 mg/ml BSA concentration in 0.1 mM sodium bicarbonate (pH 7.4) buffer and then 50 µl of FITC (1 mg/ml FITC stock in DMSO) was gently added per 1 ml of protein solution. The reaction was performed under darkness and continuous stirring for 8 h at 4 °C. To remove the excess FITC, the reaction mixture was centrifuged using a filter device (10 kDa cut off) at 5,000 rpm for 10 min. We repeated the centrifugation with nanopure water for up to five washes. The labeled DDS were freeze-dried for further use.

2.6.2 DDS uptake visualization.

A549 cells were seeded in 8-well cover slip plates with a density of 10,000 cells/well and incubated for 24 h in supplemented culture media (DMEM). Then, A549 cells were incubated with DDS and controls for 24 h. Afterwards, the A549 cells were washed with PBS 1X and fixed for 15 minutes with a 3.7% formaldehyde solution at 37 °C. After removing the fixing solution, wells were washed twice with PBS 1X followed by incubation at room temperature for 15 min of DAPI nuclear stain and Vybrant DiO dye solutions. Plates were stored at 4 °C until further analysis. The plates were observed by confocal microscopy using a Nikon Eclipse Ti microscope and 60x objective. FITC was excited at 487 nm and

monitored at 525 nm; DAPI was excited at 402 nm, and the emission was observed at 420-480 nm; Vybrant DiO was excited at 484 nm, and the emission was observed at 501 nm. Fluorescence intensity was analyzed using the NIS-Elements Viewer program (version 5.21 64-bit).

2.7 Flow cytometry analysis

Flow cytometry was implemented to analyze several cellular events involving metabolic pathways. In general, cells were seeded in a 6-well plate at a density of 10,000 cells/well and incubated for 24 h in DMEM medium containing L-glutamine, 10% FBS, and 1% penicillin/streptomycin at 37 ℃ in 5% CO_2. After 24 h, A549 cells were treated with DDS samples and controls, followed by each manufacturer protocol. The flow cytometer instrument used was a Guava® Muse® Cell Analyzer.

2.7.1 Cell cycle arrest

For the cell cycle assay (Luminex MCH100106), we followed the manufacturer's protocol. Briefly, after A549 cells were incubated with treatments for 24 h, the medium was discarded and cells were scraped, and centrifuged. The pellet was mixed with cold 70% ethanol and centrifuged for fixing. Afterwards, the pellet was washed, suspended in the cell cycle reagent, incubated for 30 min, and measured after mixing.

2.7.2 Multi-caspase activation

The multi caspase assay (Luminex MCH100109) was performed following the manufacturer's protocol. After the treatment incubation, A549 cells were scraped, and centrifuged. The pellet was dissolved in the assay buffer provided by the kit, and the working solution was incubated for 30 min at 37 ℃ in a 5% CO_2 atmosphere. Afterwards, a caspase working solution was added and incubated for 5 min at room temperature for measurement.

2.7.3 DNA damage induction

The DNA damage assay (Luminex MCH200107) was performed following the manufacturer's protocol. After the treatment incubation, A549 cells were scraped and centrifuged. The pellet was dissolved in the assay buffer provided by the kit. Later, fixation buffer was added and incubated for 10 min. Afterwards, the centrifuged pellet was dissolved in permeabilization buffer (also provided with the kit) and incubated for another 10 min. Then, the permeabilization buffer was discarded after centrifugation, and the antibody cocktail was added and incubated for 30 min. Next, the solution was washed with assay buffer and suspended in fresh assay buffer for measuring.

2.7.4 Oxidative stress production

The oxidative stress assay (Luminex MCH100111) was performed following the manufacturer's protocol. After A549 cells were treated for 24 h, the cells were scraped and centrifuged to add the reagents from the kit, incubated for 30 min and washed to be measured in the Cell Analyzer.

2.7.5 EGFR expression

The EGFR assay (Luminex MCH200102) was performed following the manufacturer's protocol. After the treatment incubation, A549 cells were scraped, and centrifuged. The pellet was dissolved in the assay buffer provided in the kit. Later, the fixation buffer was

added and incubated for 5 min. Afterwards, the centrifuged pellet was dissolved in permeabilization buffer (also provided by the kit) and incubated for another 5 min. The permeabilization buffer was discarded after centrifugation and the antibody cocktail was added and incubated for 30 min. Next, the solution was washed with assay buffer and suspended in fresh assay buffer for measuring

2.8 Statistical Analysis

All experiments were performed at least in triplicate. All data were expressed by plotting values with an average of four to eight measurements for each treatment condition as mean ± standard deviation (SD). Quantitative data were analyzed with the statistical software GraphPad Prism 9. Statistical analysis was performed using one-way analysis of variance (ANOVA) to compare the mean value of each condition versus the control. Significant differences between the means were accepted when the p-value was lower than 0.05 (*), 0.01 (**), and 0.001 (***).

3. Results

3.1 Preparation and characterization of BSA-(BeA+ Dox) DDS

The preparation of the protein-based DDS NPs was achieved using an oil-in-water-like emulsion system where the drugs were dissolved in the organic solvent DMF and added to an aqueous BSA solution. The hydrophobicity of BeA contributed to the self-assembly formation of the DDS. Many conditions were varied, such as protein-drug ratios, incubation times and whether to incorporate a lipid coating to improve nanoparticle stability. Also, our DDS was also prepared and characterized with just one drug (Dox or BeA) to compare with the DDS loaded with two drugs.
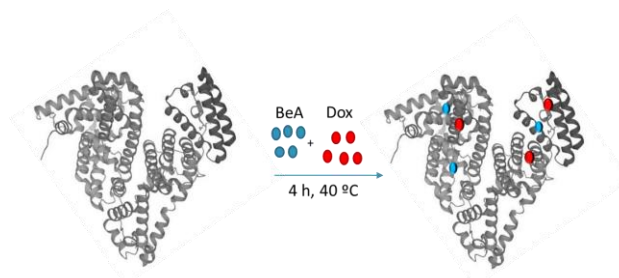
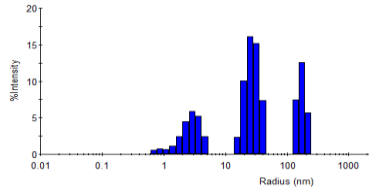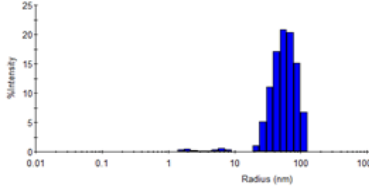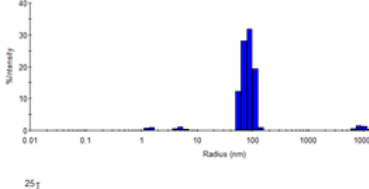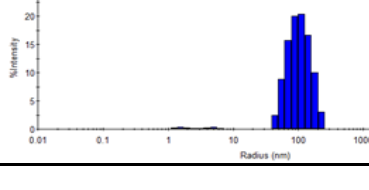Scheme 1. Illustration of the preparation of BSA(BeA+Dox)

3.1.1 Size and charge of the DDS

The properties of the DDS were characterized to identify the best conditions in terms of size and polydispersity. These properties are important for the therapeutic success and tumor accumulation of any DDS directed towards solid tumors [28]. The diameter size, surface charge (z-potential) and polydispersity index of the DDS particle were determined by DLS (**Table 1**). All developed DDS showed particle sizes in the nanometer range. The BSA-BeA DDS showed the smallest diameter (size: 97 ± 1 nm, polydispersity: 27 ± 2%), followed by BSA-Dox (size: 138 ± 13 nm, polydispersity: 51 ± 14 %), and BSA(Dox+BeA) (size: 181 ± 2 nm, polydispersity: 23.2 ± 0.4 %).

The surface charge is measured using the Zeta-potential of the NP and is relevant to dispersion stability and cellular internalization of the DDS [29]. The Zeta-potential value can be related to particle stability due to the representation of the electrostatic force around the particle and the tendency to aggregation [30][31]. Even when positive charged NPs are favored for higher internalization in the literature, there are many studies using neutral and negative NPs that have shown high internalization [32, 33]. The Zeta-

potential for all the BSA DDS with one drug (BSA-BeA: -4.6 ± 0.4, BSA-Dox: -3 ± 1) and with two drugs (BSA(BeA+Dox): -2.7 ± 0.7) were quite similar.

Table 1: Characterization of the protein-based drug delivery system by DLS.

DDS	Z-Potential (mV)	%PDI	Size (hydro-dynamic radius, nm)	DLS graph
BSA	-16 ± 5	57 ± 0	71 ± 14	
BSA - BeA	-4.6 ± 0.4	27 ± 2	97 ± 1	
BSA - Dox	-3 ± 1	51 ± 14	138 ± 13	
BSA(BeA+Dox)	-2.1 ± 0.7	23.2 ± 0.4	181 ± 2	

3.1.2 Encapsulation efficiency (EE) of BeA and Dox

A vanillin-sulfuric acid method was implemented to quantify the total amount of the triterpene BeA in the DDS. The concentration of BSA and Dox in the DDS was determined using Bradford assay and Dox intrinsic absorbance at 485 nm, respectively (**Table 2**). Those values were used to calculate the amount of each component in the DDS and, subsequently, the % EE for each drug and carrier yield (**Table 3**). The BSA-BeA DDS contained 18 ± 6 µM of BeA and 77 ± 11 µM of BSA. BSA-Dox DDS had 43 ± 6 µM of Dox and 131 ± 24 µM of BSA. Remarkably, BSA(Dox+BeA) showed the highest concentration for both drugs (61 ± 6 µM Dox and 27 ± 14 µM BeA) in 110 ± 3 µM of BSA in comparison to one-drug component DDS. Furthermore, these quantifications were used to obtain the drug EE in the NPs. The tendency observed in the drug concentrations in each DDS was very similar for the EE and the carrier yield, where BSA(Dox+BeA) showed the highest %EE (18 ± 4 % for BeA and 77 ± 15 % for Dox) and carrier yield (80 ± 12 %).

Table 2: DDS component quantification

DDS	[BSA] (µM)	[Dox] (µM)	[BeA] (µM)
BSA - BeA	77 ± 11	-	18 ± 6
BSA - Dox	131 ± 24	43 ± 6	-
BSA(BeA+Dox)	110 ± 3	61 ± 6	28 ± 12

Table 3. DDS encapsulation efficiency and carrier yield

DDS	EE (%)		Carrier yield (%)
	BeA	Dox	BSA
BSA-BeA	10 ± 2	/	58 ± 2
BSA-Dox	/	53 ± 7	37 ± 5
BSA(BeA+Dox)	18 ± 4	77 ± 15	80 ± 12

3.1.3 Circular dichroism (CD) analysis

To determine the perturbation on the structure of BSA in the formation of the DDS NPs, its secondary structure was observed through circular dichroism (CD). Also this analysis can be used to confirm the drugs (BeA and Dox) loading into the BSA cavities throughout secondary structure changes. The structural patterns of native BSA and after drug (BeA and Dox) loading were determined and shown in **Figure 1**. All the samples were analyzed using the same concentration (0.5 mg/mL). For the secondary structure, we can appreciate a similar tendency pattern but with less intensity. This decrease is more notorious for the DDS loading two drugs. The change in secondary structure spectra (190-250 nm) increases when BeA and Dox are bound to BSA. At 200 nm, the absorbance decreases, which corresponds to the protein backbone at the absorption of a cyclic ring. The decrease was considered because of configurational changes due to the increase of α-helix content [34].
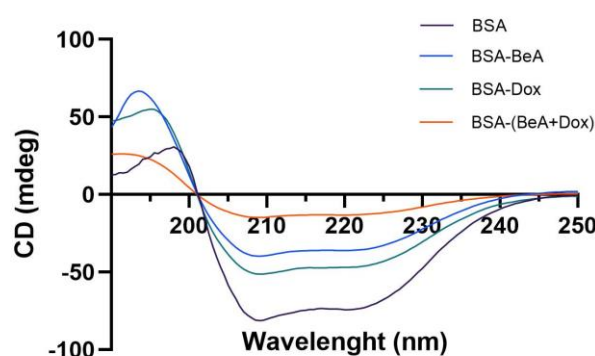

Figure 1. CD analysis of BSA-based DDS NPs. The secondary structure spectrum of BSA, BSA-BeA, BSA-Dox, and BSA-(BeA+Dox) are presented.

3.1.4 Cumulative drugs release profile

In a DDS, the drug release responding to an external stimulus is a key property to increase the drug specificity and decrease toxic side effects [35]. In this way, the cumulative Dox and BeA release profile was acquired by incubating our DDS loading the two drugs at 37 ºC in the most abundant physiological buffer, sodium bicarbonate (25 mM) at normal

plasma pH 7.4 and at a more acidic pH 6.8 to mimic the tumor micro environment. Results of the cumulative release are shown in **Figure 2**. Our system (BSA(Dox+BeA)) at pH 7.4 showed a low initial burst (~16% for both drugs) in the first hour (**Figure 2 A & B zoom inset pH 7.4**). The initial burst at pH 6.8 was drastically increased for BeA, while it remained quite similar for Dox (**Figure 2 A & B zoom inset pH 6.8)**. At pH 6.8, 52.4 ± 0.7 % of Dox and 62 ± 1 % of BeA was released within 24 h. A release in which the DDS can accumulate in the tumor followed by fast drug release is desired, At pH 7.4, the release was significantly slower and within 24 h 28.9 ± 0.7 % of Dox was released and 38.8 ± 0.4 % of BeA. At pH 6.8, both agents were fully released from the DDS after 72 h. In contrast, at pH 7.4, BeA and Dox were fully released at 96 h and 144 h, respectively. A faster release in the tumor micro environment is a desired property.
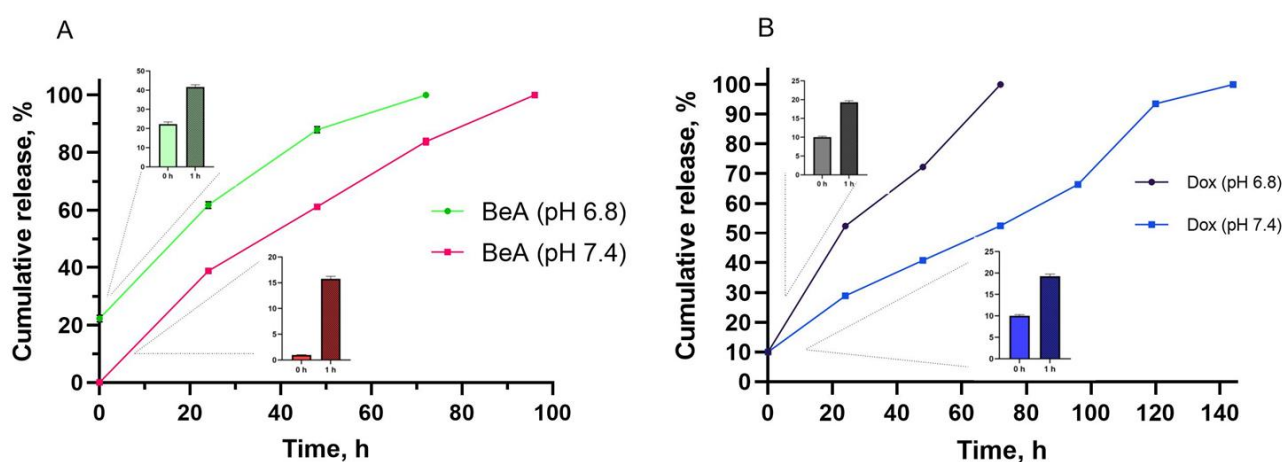

Figure 2: Cumulative in vitro release of the encapsulated drugs BeA (A) and Dox (B) from the DDS. The insets represent the initial burst release of each drug at 0 and 1 h insets. DDS was incubated in sodium bicarbonate buffer (pH 6.8 and 7.4) at 37 ºC and sink conditions were maintained. All data are represented as mean ± SD.

3.2 In vitro assays

The following in vitro assays were performed with A549 cells. To allow for comparison with normal non-cancerous cells, MRC5 fibroblast cells were used. In the mechanistic assays, only A549 cell were used. The incubation time was 24 h and the drug concentrations employed were the initially determined IC_{50} values. Native fatty acid-free BSA was used as a negative control for all the in vitro assays.

3.2.1 Cytotoxicity of BeA and Dox in A549 cells

A dose-response curve was created for A549 cells to confirm each drug's ability to induce cell death. Each drug was incubated at several μM concentrations for 24 h in a confluency of 1×10^4 cells/well to obtain the IC_{50} using MTS viability assay. The IC_{50} values obtained were 98 ± 18 μM for Dox and 42 ± 2 μM for BeA (**Figure 3**). As expected, cell viability decreases at increasing drug concentration. Then, A549 cells were co-incubated with both drugs, a slightly decrease (25 ± 2 μM BeA and 86 ± 1 μM Dox) in the IC_{50} concentration of each drug from this Dox + BeA combination (**Figure 4**).
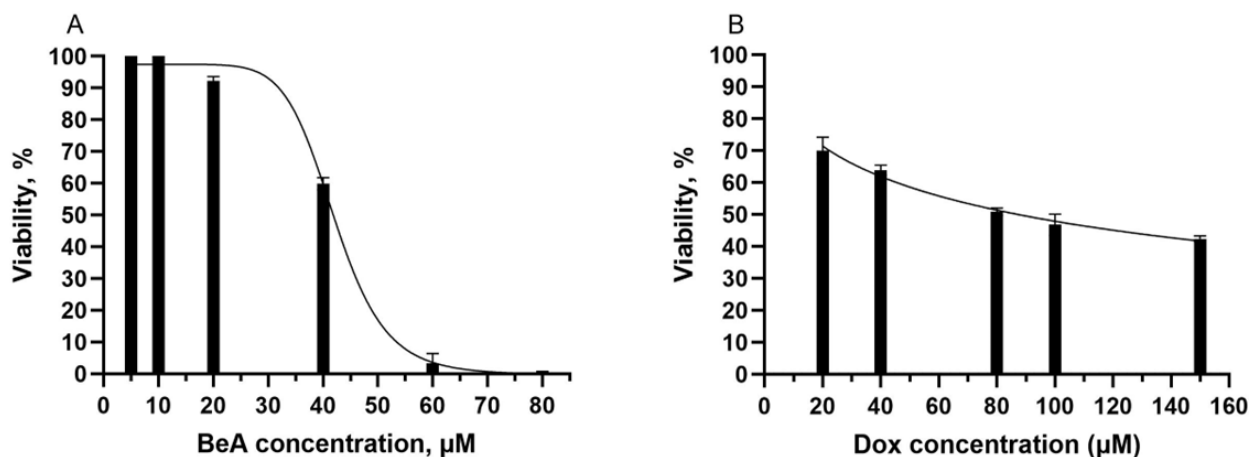
Figure 3:   Viability of A549 cells incubated with different concentrations of BeA (A) and Dox (B) determined by MTS assay. All data are represented as mean ± SD
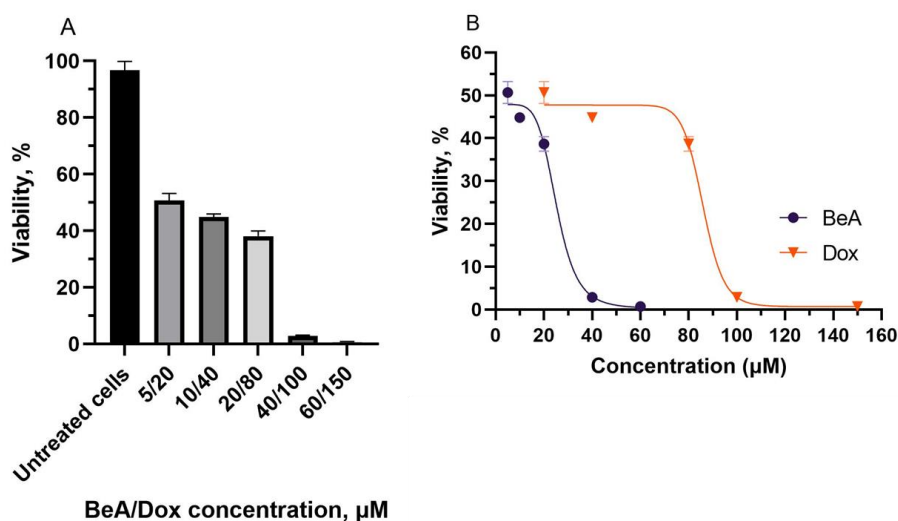

Figure 4:   Cell viability of BeA and Dox co-incubation. (A) Viability of A549 cells simultaneously incubated with a range of concentrations of BeA and Dox determined by MTS assay. (B) Dose response curve of BeA and Dox in the drug combination. All data are represented as mean ± SD.

3.2.2 Molecular interaction effect of the BeA and Dox combination

Because we determined a decrease in the IC_{50} of the drugs BeA and Dox combined, We decided to use the CompuSyn software to quantitatively analyze the molecular interaction effect of BeA and Dox and calculate the combination index (CI) values using the Chou and Talalay equation [26]. The mean CI value obtained was 0.73 ± 0.2, indicating a synergistic effect (< 1) of the drug combination against A549 cells. We also used Synergy Finder 2.0, a web application for the analysis of drug combination screening [27], to calculate the synergy score of the drug combination to confirm the results from the CompuSyn. The synergy score was 19.06 (where >10 indicates synergistic effect) (**Figure 5**). This score can be interpreted as the average excess response due to drug interactions (i.e., synergy score of 19.06 corresponds to 19.05% of response beyond expectation), revealing that the combination of BeA and Dox exhibits a synergistic effect on the viability of A549 cells. The more synergistic area score is 34.46, shown in the gray highlighted square of **Figure 5A**, when the concentrations are 40 µM and 100 µM for BeA and Dox, respectively.
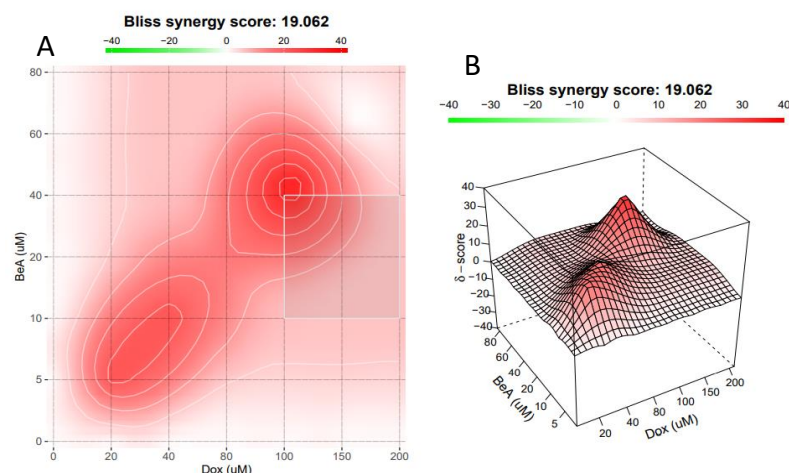
Figure 5: Synergy distribution (A) and 2D surface plot (B) of dose-response analysis using the Bliss method in A549 cells treated with BeA and Dox simultaneously. Synergy Finder 2.0 software was used for this analysis.

3.2.3 Cytotoxicity of the BSA(Bea+Dox) DDS

After we confirmed that the combination of BeA and Dox worked synergistically together, we tested our BSA-(BeA+Dox) DDS to determine its effect against NSCLC A549 cells. Once the DDS were prepared and characterized, A549 cells were treated with a range of concentrations for 24 h and 48 h (**Figure 6**). The highest concentration of drugs loaded in the DDS (25.5 μM Dox and 13.0 μM BeA), reduced the viability to 42 ± 2 % after 24 h and to 5.9 ± 0.8 % after 48 h of treatment. Normal lung fibroblast MRC5 cells were also treated with the DDS. Cell viability was 58.0 ± 0.4 % after 24 h and 0.5 ± 0.4 % after 48 h. This means that, when employing isolated cells, any growing cell is impacted by the drugs, as expected. One has to keep in mind, however, that passive accumulation of the nanosized DDS under in vivo conditions should reduce the impact on healthy cells in the real treatment. This in general is the idea of nanosized systems loaded with cytotoxic drugs.

Then, the IC_{50} values of each drug in the DDS was calculated. When the DDS contains 13 ± 3 μM of BeA and 27 ± 6 μM of Dox, the cell viability of A549 cell reached 50%. This implies that the IC_{50} of BeA and Dox are significantly lower in the BSA(BeA+Dox) DDS than the naked drugs individually and also in combination. In addition, when MRC5 cells were treated with BSA(Bea+Dox) DDS, we observed a slightly less cytotoxic effect in comparison to A549 cancer cells after 24h incubation, but an even larger effect after 48 h (Figure 6).
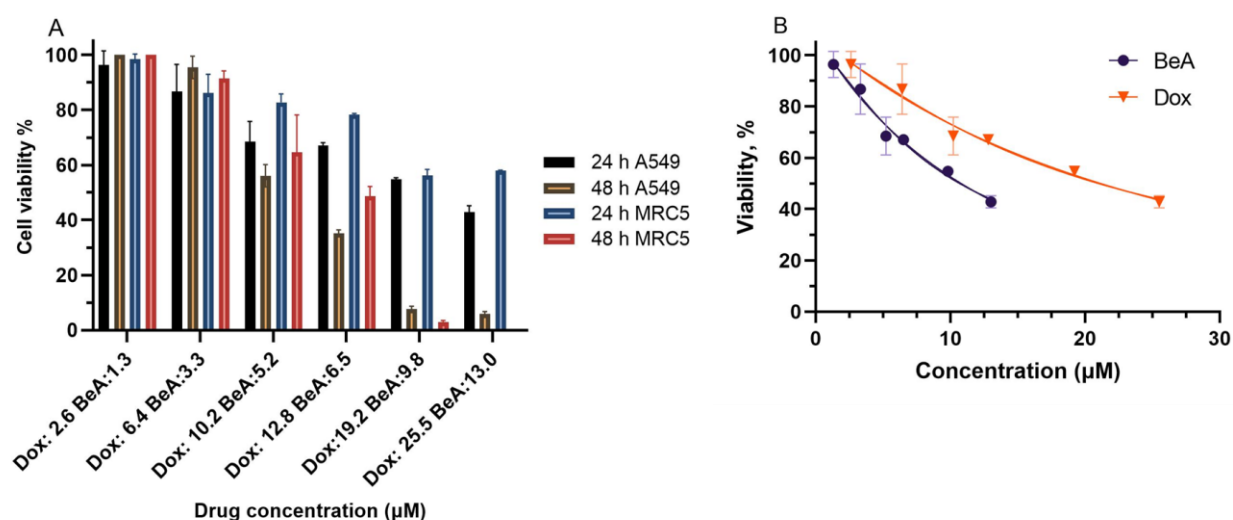
Figure 6: Cell viability of BSA-(BeA+Dox). (A) A549 and normal lung fibroblast MRC5 cells were incubated with a range of concentrations of the BSA(BeA+Dox) DDS. (B) Dose-response curves to determine the IC_{50} of BeA and Dox in the DDS against A549 cells. BSA (carrier) concentration was from 5 to 54 µM, showing no cytotoxicity.

3.2.4 Cellular internalization of the BSA(Dox+BeA) DDS

A549 cells were grown on chambered slides and incubated with the FITC-labeled DDS for 24 h to trace the specific cellular internalization of the system. DAPI dye (blue fluorescence) was used to stain cell nuclei, Dox intrinsic fluorescence was observed as red fluorescence, and Vybrant Dio dye (green fluorescence) was used to stain the cellular membrane. After the A549 cells were treated with the samples, considerable amounts of BSA(Dox+BeA) were internalized and observed in the membrane areas and the cell nucleus, respectively (**Figure 7 B**). In addition, as a DNA intercalator, Dox was colocalized with cell nuclei [5] (**Figure 7 B and D).**
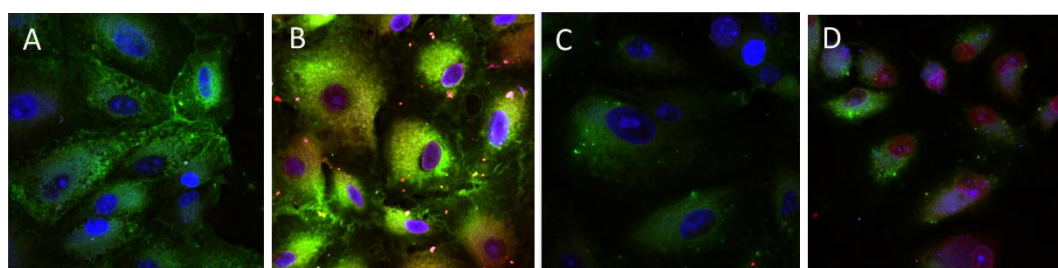

Figure 7: Confocal microscopy images after incubation of A459 cells with the FTIC labeled DDS. From A-B, samples were modified with FITC (green fluorescence) to visualize cellular uptake in A549 cells, DAPI (blue fluorescence) was used to stain cell nucleus and the red signal is from the Dox fluorescence. Cells were incubated with (A) 10 µM free FITC as control, (B) FITC-labeled BSA(Dox+BeA) DDS. In C and D cells were stained with Vibrant Dio dye (green fluorescence) to visualize the cell membrane, with DAPI to stain the nucleus and the red signal is from Dox fluorescence. Cells were incubated with (C) just Vibrant Dio and DAPI, (D) the former and BSA(Dox+BeA) for 24 h.

In images B and D, where the cells were treated with BSA(Dox+BeA), quenching of the blue and red dyes is common due to Dox and DAPI binding to similar areas of the DNA in the nucleus [36].

3.3 Flow cytometry analysis

Using the IC_{50} of the drugs delivered via DDS as reference, we selected to use the preparation that contains 5.2 µM of BeA and 10.2 µM of Dox (~IC_{50}/2) at 24 h of incubation in A549 cells for the remainder of the mechanistic experiments. As negative control, we used 50 µM fatty acid depleted-BSA. As positive controls, we used the free drugs at 20 µM of BeA and 20 µM of Dox.

3.3.1 Effect of BSA(Bea+Dox) DDS on the cell cycle

Cell cycle is an ordered sequence of events to prepare for cell growth and division. In G0, a cell is in a resting or quiescent stage and then, it can enter to the cell cycle phases, where the cell has a size increase (G1 phase), synthesize DNA (S-phase), synthetize proteins for cell division (G2-phase) and finally the cell divides by mitosis (M-phase) [37]. **Figure 8** summarizes the results of cell cycle analysis by flow cytometry. Treatment with 20 µM of free BeA did not cause significant changes in the cell cycle phases compared to untreated cells, where the highest population was in the G0/G1 phase. This could mean that BeA induced cell cycle arrest at G0/G1 phase, as demonstrated in the literature [38]. Meanwhile, Dox showed 51.4% G0/G1, 44.0% S, and 4.3 % G2/M, showing a marked increase in cells in the S-phase. Exposure of the cells to the BSA(BeA+Dox) DDS caused an even more remarkable increase of cells in S-phase (50.9%). From the literature, Dox revealed cell proliferation inhibition through cell cycle arrest at the S- and G2/M- phases in a kidney cell line [39, 40].

3.3.2 Effect of BSA(Bea+Dox) on caspase activity

Caspases are cysteine proteases that executes apoptosis (intrinsic and extrinsic programmed cell death). Dox can induce apoptosis through caspases activation [41][42]. Untreated A549 cells registered a total caspase activation of 57.2%. Treating the cells with the free drugs caused 68.3% activation in case of BeA, and 97.4% in case of Dox 97.4%, respectively. An even higher level of caspase activation (99.3%) was caused by exposure to the BSA(BeA+Dox) DDS. Comparison of the DDS with the free anticancer drugs (BeA and Dox) revealed a slight advantage of the DDS in caspase activation and cell death (**Figure 9**).
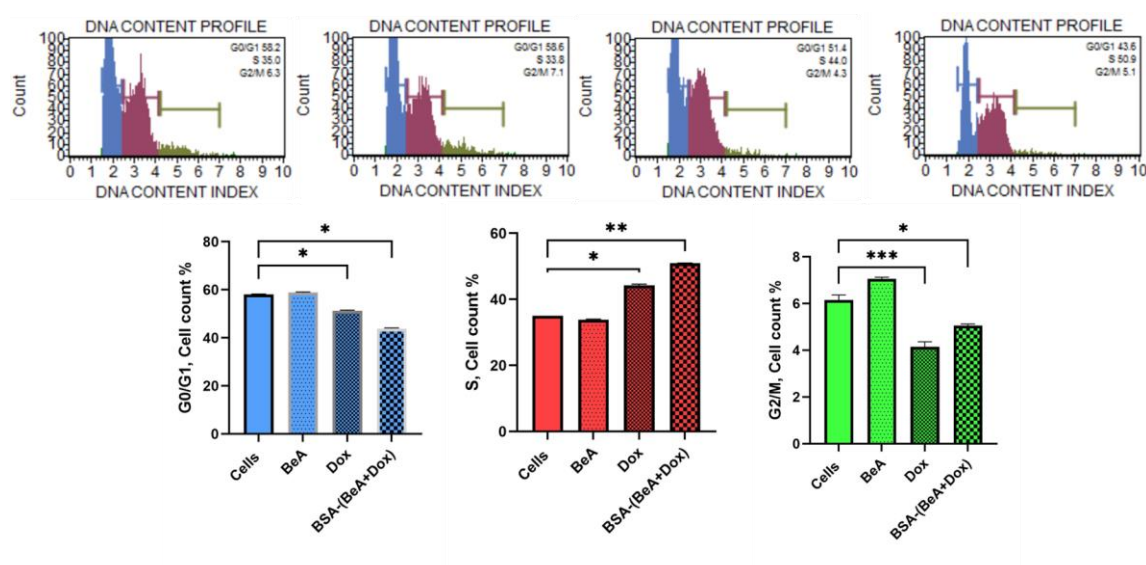

Figure 8. Cell cycle index induced by treatment of A549 cells with BSA(BeA+Dox). The cell cycle distribution of untreated A549 cells (A) and cells treated with BeA (B), Dox (C), and BSA(Bea + Dox) (D) is presented. Comparison of cell populations in G0/G1 (E), S (F), and G2/M (G) phases of A549 cells for each sample are shown in (A)-(D). Data were shown as mean ± SD and statistical significance is indicated.
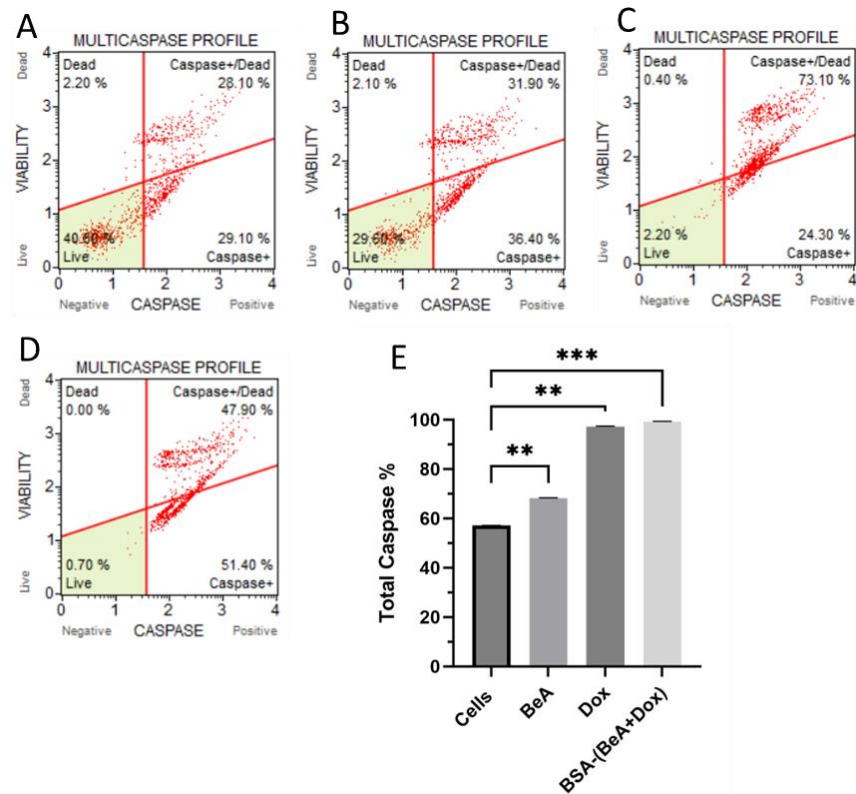
Figure 9. Activation of caspases by BSA(Bea+Dox). The percentage and distribution of cells exhibiting caspase activity; (A) untreated A549 cells, and cells treated with BeA (B), Dox (C), and BSA(Bea+Dox) (D). Data are presented as the means ± SD and statistical significance for all treated cells versus the control is indicated.

3.3.3 Effect of BSA(Bea+Dox) on the DNA processing machinery

DNA damage frequently affects the function of genes encoded [43]. DNA repair mechanisms are activated in the affected cell to correct the problem. Nevertheless, after a double-strand break when damage might be too severe for repair, phosphorylation of the histone variant X (H2A.X) and ataxia telangiectasia mutated (ATM) kinase is promoted leading to cell death [44]. The assay to assess the magnitude of this pathway indirectly measures double stand breaks by measuring the amount of phosphorylated H2A.X and ATM. We found that Dox induced an increase in the total DNA damage (97.04% vs 20.85% in untreated cells), while the BSA(Bea+Dox) DDS induced 92.48% (**Figure 10**). This result confirms the presence and functionality of Dox in the DDS. BeA did not show any increase in DNA damage.

3.3.4 Effect of BSA(Bea+Dox) on oxidative stress production

Perturbation in redox homeostasis can increase the concentration of reactive oxygen species (ROS) which subsequently can cause cancer development. However, drastic increments in ROS could also promote cell death [45]. Cellular ROS production was measured by intracellular detection of hydroxyl (HO*) and superoxide (O_2*) free radicals in A549 cells (**Figure 11**). BeA and Dox treated cells exhibited ROS production of 27.4% and 49.20%, respectively, compared with untreated cells. In addition, BSA-(BeA+Dox) promoted a high ROS production of 49.60%.
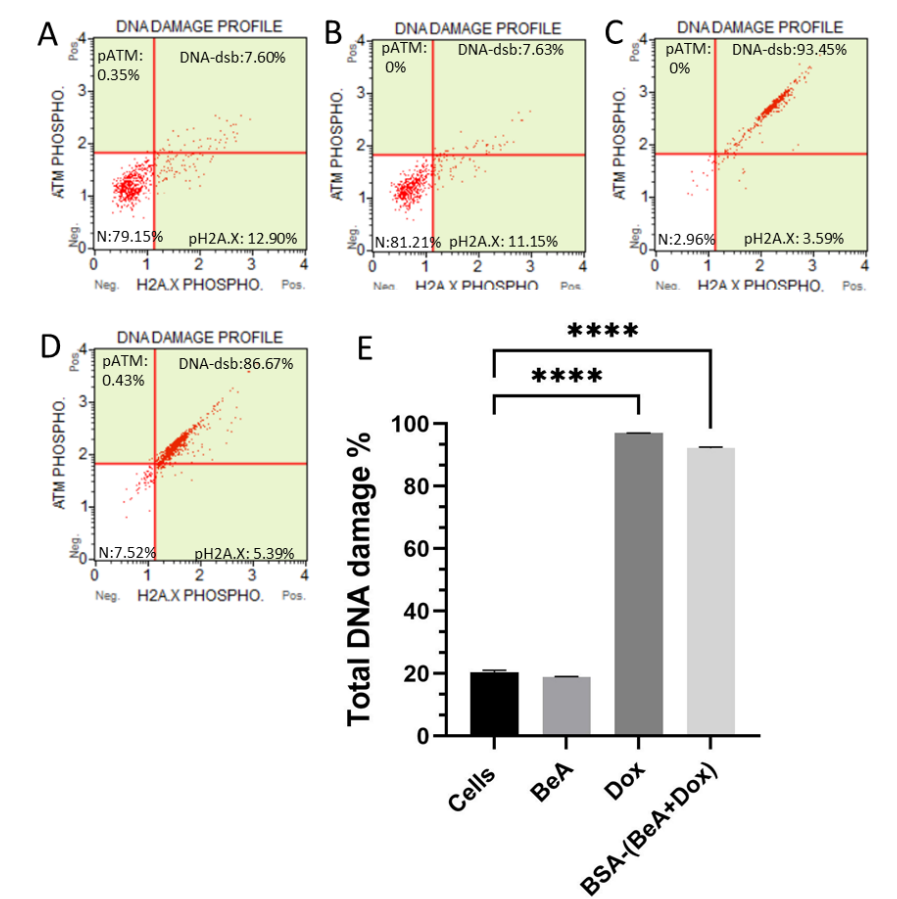
Figure 10. DNA damage determination induced by the BSA(Bea+Dox) DDS in A459 cells. The distribution of DNA damage in untreated cells (A) and cells treated with BeA (B), Dox (C), and BSA(Bea+Dox) (D) is presented. Data are presented as the means ± SD.
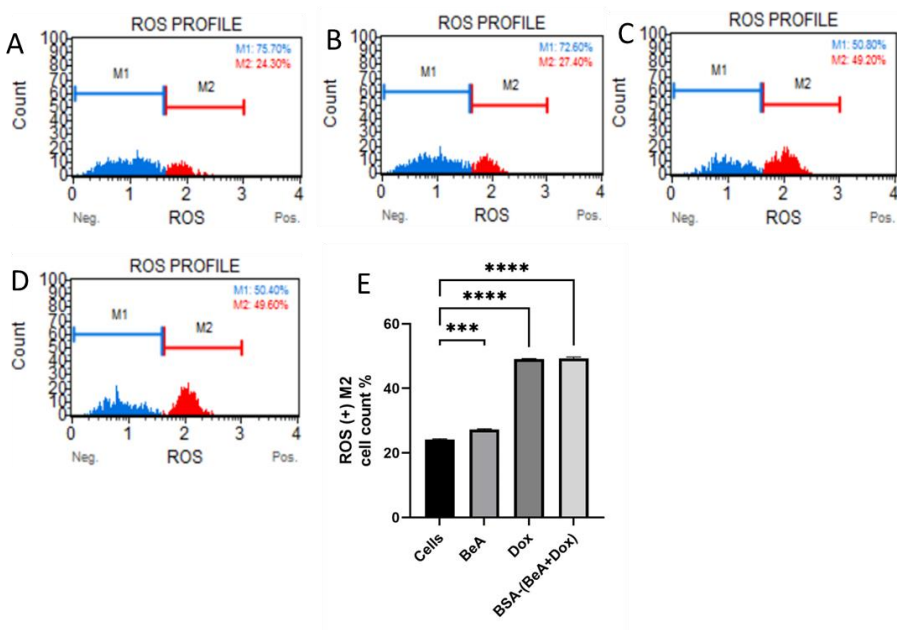

Figure 11: Histograms obtained from oxidative stress measurements of untreated and treated A459 cells. The distribution of A459 cells not producing ROS (M1) and producing ROS (M2) is shown for untreated cells (A) and cells treated with BeA (B), Dox (C), and BSA-(Bea+Dox) (D). Data are presented as the means ± SD. All treated cells were significantly different from non-treated cells.

3.3.5 Effect of BSA(Bea+ Dox) on Epidermal Growth Factor Receptor (EGFR) expression

EGFR is a transmembrane glycoprotein that is overexpressed in several cancers, especially NSCLC and it promotes cell proliferation, invasion, and chemoresistance [46]. In this study, we identified the EGFR expression by flow cytometry and show the non-expressing and expressing cells (inactivated and activated via phosphorylation). The untreated cells produced 24.0% of EGFR, whereas BeA and Dox treated cells produced 22.2% and 80.8%, respectively. Treatment of the A459 cells with the BSA(BeA+Dox) DDS produced 41.7% of EGFR. We conclude that EGFR expression was significantly decreased when BeA was combined with Dox in the BSA(BeA+Dox) DDS (**Figure 12**)
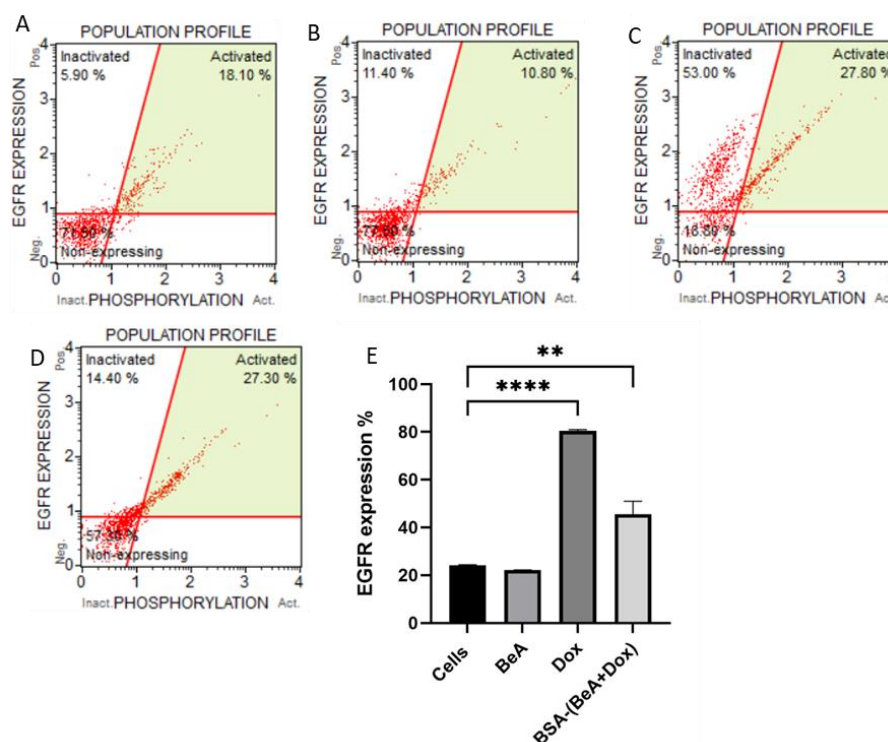

Figure 12. Determination of EGFR expression produced by treatment of A459 cells. Distribution of EGFR expression in untreated cells (A) and cells treated with BeA (B), Dox (C), and BSA(Bea+Dox) (D). Data are presented as the means ± SD.

4. Discussion

Many albumin-based NPs have been developed into DDS [47][48]. Our system, BSA(BeA+Dox) possesses properties (size and charge) that would allow for passive delivery and accumulation in tumors through the enhanced permeation and retention (EPR) effect caused by irregular tumor vasculature [20]. Furthermore, our DDS could be considered as a self-assembling complex between BSA and two molecularly different drugs (BeA and Dox). The triterpene BeA and the anthracycline Dox exposed strong interactions with the BSA structure pockets. Furthermore, the encapsulation efficiency (EE) was better when both drugs were loaded into the protein than just with one drug alone.

Previous studies of BSA using molecular dynamic simulation methods revealed how BeA [49] and Dox [50] are bound to BSA. BSA possesses large hydrophobic binding pockets on its surface. BeA binds to these large hydrophobic cavities of drug binding site I of subdomain IIA and IIB through hydrophobic and hydrogen bonding interactions [49]. The other drug, Dox, strongly binds to BSA by hydrophobic, hydrophilic, and hydrogen bonding interactions for stabilization. Those binding interactions alter the protein's secondary

structure causing partial protein destabilization [49] [50] which were registered in the CD analysis.

The term combination therapy is used when two or more drugs positively affect the drugs' pharmacodynamics interaction (i.e., additive and synergistic). The primary purpose of combination therapy is to lower drug doses so that the patients experience less side effects while the efficiency of the treatment is enhanced [51]. In our experiments a synergistic effect is revealed in the drug combination of Dox and BeA increasing the cytotoxic effect. This synergy was demonstrated by co-incubating A459 cells with free Dox and BeA and this effect was increased by the assistance of the nanosized BSA carrier

Considering that the extracellular pH in healthy tissue is 7.4, the pH in cancer tissues is more acidic (between 6.3 and 7.0) due to the dysregulation of the acid-base homeostasis in tumors [52]. BSA(BeA+Dox) DDS released the drugs faster in an acidic environment (pH 6.8) than in physiological conditions environments (pH 7.4), revealed by in vitro cumulative drug release studies adding some selectivity by this stimulus to the DDS. Under acidic conditions, the full release took 72 h, and after 24 h, the drug release was slightly higher than 50%. This tendency is also observed in cell viability studies on A549 cells at 24 h and 48 h. Confocal microscopy validated that the BSA(BeA+Dox) DDS was internalized and Dox was localized in the nucleus.

Normal cells, MRC5, were also treated with BSA(BeA+Dox) DDS. The BSA(BeA+Dox) DDS was more aggressive on cancer cells (A549) than normal cells (MRC5) after 24 h of treatment. However, when the treatment was extended for up to 48 h, the normal lung MRC5 cells also exhibited high mortality in the highest drug concentration. An important consideration about MRC5 fibroblast cells, is that MRC5 are tumor associated cells which enhance invasive migration of cancer cells promoting the Warburg effect (intensification of aerobic usage of glucose and/or lactate promoting cancer reinforcement) and contributing to chemoresistance [53, 54]. Thus, cytotoxicity to MRC5 after 48 h of treatment might provide an additional support to reduce chemoresistance.

The results from the metabolic cellular studies revealed that BSA(BeA+Dox) produce S-phase cell cycle arrest which was confirmed by the increase in DNA damage. The increase in oxidative stress through ROS could induce DNA disruption and/or mitochondrial membrane permeabilization. As a result, we found an increase in caspase activation confirming the induction of apoptotic pathways. Interestingly, the EGFR expression significantly decreased after DDS treatment, contrary to Dox alone. The BSA(BeA+Dox) DDS might provide an alternative to diminish and evade multidrug chemo-resistance in lung cancer patients.

5. Conclusions

Novel BSA-based NPs were developed with the capacity to incorporate lipophilic (i.e., BeA) and hydrophilic moieties (i.e., Dox). The BSA(BeA+Dox) DDS has the characteristics of size and charge suitable for passive delivery into lung tumors and to be internalized by NSCLC cells. The surface charge of the DDS NP was slightly negative, and this property has shown to prolong circulating half-life and accumulation in tumors. Besides the synergistic effect of BeA and Dox combination, BSA(BeA+Dox) DDS diminished the expression of EGFR commonly produced in NSCLC by chemotherapeutic agents as Dox. BSA(BeA+Dox) has the potential to increase the bioavailability of Dox and BeA and decrease chemoresistance during intravenous administration. Further studies of drug combination DDS must be continued to explore anticancer efficacy for in vivo studies.

.

References

1. Figueroa, C.M., et al., *Smart Release Nano-formulation of Cytochrome C and Hyaluronic Acid Induces Apoptosis in Cancer Cells.* J Nanomed Nanotechnol, 2017. **8**(1).

2. López-González, A., et al., *The role of anthracyclines in small cell lung cancer.* Annals of translational medicine, 2013. **1**(1).

3. Rathos, M.J., et al., *Potentiation of in vitro and in vivoantitumor efficacy of doxorubicin by cyclin-dependent kinase inhibitor P276-00 in human non-small cell lung cancer cells.* Bmc Cancer, 2013. **13**(1): p. 1-10.

4. Christowitz, C., et al., *Mechanisms of doxorubicin-induced drug resistance and drug resistant tumour growth in a murine breast tumour model.* BMC cancer, 2019. **19**(1): p. 1-10.

5. Ijäs, H., et al., *Unraveling the interaction between doxorubicin and DNA origami nanostructures for customizable chemotherapeutic drug release.* Nucleic acids research, 2021. **49**(6): p. 3048-3062.

6. Kaowinn, S., et al., *Increased EGFR expression induced by a novel oncogene, CUG2, confers resistance to doxorubicin through Stat1-HDAC4 signaling.* Cellular Oncology, 2017. **40**(6): p. 549-561.

7. Yu, X., et al., *GSH-responsive curcumin/doxorubicin encapsulated Bactrian camel serum albumin nanocomposites with synergistic effect against lung cancer cells.* Journal of Biomedical Research, 2020. **34**(1): p. 54.

8. Suresh, C., et al., *New ionic derivatives of betulinic acid as highly potent anti-cancer agents.* Bioorganic & medicinal chemistry letters, 2012. **22**(4): p. 1734-1738.

9. Oliveira-Costa, J.F., et al., *Anti-Inflammatory Activities of Betulinic Acid: A Review.* Frontiers in Pharmacology, 2022: p. 1866.

10. Jiang, W., et al., *Betulinic acid in the treatment of tumour diseases: Application and research progress.* Biomed Pharmacother, 2021. **142**: p. 111990.

11. Bravo-Alfaro, D.A., et al., *Self-nanoemulsifying drug delivery system (SNEDDS) improves the oral bioavailability of betulinic acid.* Journal of Molecular Liquids, 2022. **364**: p. 119946.

12. Saneja, A., et al., *Therapeutic applications of betulinic acid nanoformulations.* Annals of the New York Academy of Sciences, 2018. **1421**(1): p. 5-18.

13. Lehár, J., et al., *Synergistic drug combinations tend to improve therapeutically relevant selectivity.* Nature biotechnology, 2009. **27**(7): p. 659-666.

14. Yin, N., et al., *Synergistic and antagonistic drug combinations depend on network topology.* PloS one, 2014. **9**(4): p. e93960.

15. Karami, K., et al., *BSA nanoparticles as controlled release carriers for isophethalaldoxime palladacycle complex; synthesis, characterization, in vitro evaluation, cytotoxicity and release kinetics analysis.* New Journal of Chemistry, 2020. **44**(11): p. 4394-4405.

16. Topală, T., et al., *Bovine serum albumin interactions with metal complexes.* Clujul medical, 2014. **87**(4): p. 215.

17. Motevalli, S.M., et al., *Co-encapsulation of curcumin and doxorubicin in albumin nanoparticles blocks the adaptive treatment tolerance of cancer cells.* Biophysics Reports, 2019. **5**(1): p. 19-30.

18. Prajapati, R., E. Garcia-Garrido, and Á. Somoza, *Albumin-based nanoparticles for the delivery of doxorubicin in breast cancer.* Cancers, 2021. **13**(12): p. 3011.

19. Yuan, H., et al., *Albumin nanoparticle of paclitaxel (Abraxane) decreases while taxol increases breast cancer stem cells in treatment of triple negative breast cancer.* Molecular pharmaceutics, 2020. **17**(7): p. 2275-2286.

20. Molina, A.M., et al., *Redox-sensitive cross-linking enhances albumin nanoparticle function as delivery system for photodynamic cancer therapy.* J Nanomed Nanotechnol, 2016. **6**(3).

21. Delgado, Y., et al., *Development of HAMLET-like cytochrome c-oleic acid nanoparticles for cancer therapy.* Journal of Nanomedicine & Nanotechnology, 2015. **6**(4): p. 1.

22. Kielkopf, C.L., W. Bauer, and I.L. Urbatsch, *Bradford assay for determining protein concentration.* Cold Spring Harbor Protocols, 2020. **2020**(4): p. pdb. prot102269.

23. Shah, S., et al., *Fluorescence properties of doxorubicin in PBS buffer and PVA films.* Journal of Photochemistry and Photobiology B: Biology, 2017. **170**: p. 65-69.

24. Hiai, S., H. Oura, and T. Nakajima, *Color reaction of some sapogenins and saponins with vanillin and sulfuric acid.* Planta Med, 1976. **29**(2): p. 116-22.

25. Morales-Cruz, M., et al., *Two-step nanoprecipitation for the production of protein-loaded PLGA nanospheres.* Results Pharma Sci, 2012. **2**: p. 79-85.

26. Chou, T.C. and P. Talalay, *Quantitative analysis of dose-effect relationships: the combined effects of multiple drugs or enzyme inhibitors.* Adv Enzyme Regul, 1984. **22**: p. 27-55.

27. Ianevski, A., A.K. Giri, and T. Aittokallio, *SynergyFinder 2.0: visual analytics of multi-drug combination synergies.* Nucleic acids research, 2020. **48**(W1): p. W488-W493.

28. Decuzzi, P., et al., *Size and shape effects in the biodistribution of intravascularly injected particles.* Journal of Controlled Release, 2010. **141**(3): p. 320-327.

29. Augustine, R., et al., *Cellular uptake and retention of nanoparticles: Insights on particle properties and interaction with cellular components.* Materials Today Communications, 2020. **25**: p. 101692.

30. Larsson, M., A. Hill, and J. Duffy, *Suspension stability; why particle size, zeta potential and rheology are important.* Annual transactions of the Nordic rheology society, 2012. **20**(2012): p. 6.

31. Clogston, J.D. and A.K. Patri, *Zeta potential measurement*, in *Characterization of nanoparticles intended for drug delivery.* 2011, Springer. p. 63-70.

32. Murugan, K., et al., *Parameters and characteristics governing cellular internalization and trans-barrier trafficking of nanostructures.* International journal of nanomedicine, 2015. **10**: p. 2191.

33. Harush-Frenkel, O., et al., *Surface charge of nanoparticles determines their endocytic and transcytotic pathway in polarized MDCK cells.* Biomacromolecules, 2008. **9**(2): p. 435-443.

34. Sun, C., et al., *Unfolding and refolding of bovine serum albumin induced by cetylpyridinium bromide.* Biophysical journal, 2005. **88**(5): p. 3518-3524.

35. Pham, S.H., Y. Choi, and J. Choi, *Stimuli-responsive nanomaterials for application in antitumor therapy and drug delivery.* Pharmaceutics, 2020. **12**(7): p. 630.

36. Lee, C., et al., *Modulating the chemo-mechanical response of structured DNA assemblies through binding molecules.* Nucleic acids research, 2021. **49**(21): p. 12591-12599.

37.   Nasmyth, K., *Putting the cell cycle in order.* Science, 1996. **274**(5293): p. 1643-1645.

38.   Li, Y., et al., *Betulinic acid self-assembled nanoparticles for effective treatment of glioblastoma.* Journal of nanobiotechnology, 2022. **20**(1): p. 1-13.

39.   Park, E.-J., et al., *Doxorubicin induces cytotoxicity through upregulation of perk–dependent ATF3.* 2012.

40.   Kim, H.-S., Y.-S. Lee, and D.-K. Kim, *Doxorubicin exerts cytotoxic effects through cell cycle arrest and Fas-mediated cell death.* Pharmacology, 2009. **84**(5): p. 300-309.

41.   Gamen, S., et al., *Doxorubicin treatment activates a Z-VAD-sensitive caspase, which causes Δψm loss, caspase-9 activity, and apoptosis in Jurkat cells.* Experimental cell research, 2000. **258**(1): p. 223-235.

42.   Fulda, S., *Betulinic acid for cancer treatment and prevention.* International journal of molecular sciences, 2008. **9**(6): p. 1096-1107.

43.   Martin, L.J., *DNA damage and repair: relevance to mechanisms of neurodegeneration.* Journal of Neuropathology & Experimental Neurology, 2008. **67**(5): p. 377-387.

44.   Podhorecka, M., A. Skladanowski, and P. Bozko, *H2AX phosphorylation: its role in DNA damage response and cancer therapy.* Journal of nucleic acids, 2010. **2010**.

45.   Perillo, B., et al., *ROS in cancer therapy: The bright side of the moon.* Experimental & Molecular Medicine, 2020. **52**(2): p. 192-203.

46.   Luo, Y.-H. and Y.-M. Chen, *Influence of chemotherapy on EGFR mutation status.* Translational lung cancer research, 2013. **2**(6): p. 442.

47.   Elzoghby, A.O., W.M. Samy, and N.A. Elgindy, *Protein-based nanocarriers as promising drug and gene delivery systems.* J Control Release, 2012. **161**(1): p. 38-49.

48.   Sand, K.M.K., et al., *Unraveling the interaction between FcRn and albumin: opportunities for design of albumin-based therapeutics.* Frontiers in immunology, 2015: p. 682.

49.   Malleda, C., et al., *Molecular dynamics simulation studies of betulinic acid with human serum albumin.* Journal of molecular modeling, 2012. **18**(6): p. 2589-2597.

50.   Agudelo, D., et al., *Probing the binding sites of antibiotic drugs doxorubicin and N-(trifluoroacetyl) doxorubicin with human and bovine serum albumins.* 2012.

51.   Kamran, S., et al., *Diosmetin Exerts Synergistic Effects in Combination with 5-Fluorouracil in Colorectal Cancer Cells.* Biomedicines, 2022. **10**(3): p. 531.

52.   Lee, S.-H. and J.R. Griffiths, *How and why are cancers acidic? Carbonic anhydrase IX and the homeostatic control of tumour extracellular pH.* Cancers, 2020. **12**(6): p. 1616.

53.   Ding, S.-M., et al., *MRC-5 Cancer-associated Fibroblasts Influence Production of Cancer Stem Cell Markers and Inflammation-associated Cell Surface Molecules, in Liver Cancer Cell Lines.* International journal of medical sciences, 2019. **16**(8): p. 1157.

54.   Koukourakis, M.I., et al., *Metabolic cooperation between co-cultured lung cancer cells and lung fibroblasts.* Laboratory investigation, 2017. **97**(11): p. 1321-1331.